POLITECNICO DI TORINO
Repository ISTITUZIONALE

The role of spatial variations of abiotic factors in mediating intratumour phenotypic heterogeneity

Original
The role of spatial variations of abiotic factors in mediating intratumour phenotypic heterogeneity / Lorenzi, T.; Venkataraman, C.; Lorz, A.; Chaplain, M. A. J.. - In: JOURNAL OF THEORETICAL BIOLOGY. - ISSN 0022-5193. - ELETTRONICO. - 451:(2018), pp. 101-110. [10.1016/j.jtbi.2018.05.002]

Availability:
This version is available at: 11583/2870801 since: 2021-02-12T12:57:03Z

Publisher:
Academic Press

Published
DOI:10.1016/j.jtbi.2018.05.002

Terms of use:
openAccess

This article is made available under terms and conditions as specified in the corresponding bibliographic description in the repository

Publisher copyright

(Article begins on next page)

18 October 2022

The role of spatial variations of abiotic factors in mediating intratumour phenotypic heterogeneity

Tommaso Lorenzi[a,1], Chandrasekhar Venkataraman[a,1], Alexander Lorz[b], Mark A.J. Chaplain[*,a]

[a] *School of Mathematics and Statistics, University of St Andrews, St Andrews KY16 9SS, United Kingdom*

[b] *CEMSE Division, King Abdullah University of Science and Technology (KAUST), Thuwal, Saudi Arabia & Sorbonne Universités, UPMC Univ Paris 06, UMR 7598, Laboratoire Jacques-Louis Lions, Paris, France*

Abstract

We present here a space- and phenotype-structured model of selection dynamics between cancer cells within a solid tumour. In the framework of this model, we combine formal analyses with numerical simulations to investigate *in silico* the role played by the spatial distribution of abiotic components of the tumour microenvironment in mediating phenotypic selection of cancer cells. Numerical simulations are performed both on the 3D geometry of an *in silico* multicellular tumour spheroid and on the 3D geometry of an *in vivo* human hepatic tumour, which was imaged using computerised tomography. The results obtained show that inhomogeneities in the spatial distribution of oxygen, currently observed in solid tumours, can promote the creation of distinct local niches and lead to the selection of different phenotypic variants within the same tumour. This process fosters the emergence of stable phenotypic heterogeneity and supports the presence of hypoxic cells resistant to cytotoxic therapy prior to treatment. Our theoretical results demonstrate the importance of integrating spatial data with ecological principles when evaluating the therapeutic response of solid tumours to cytotoxic therapy.

Key words: Intratumour heterogeneity, Phenotypic selection, Mathematical oncology, Partial differential equations, Finite element methods

[*]Corresponding author; *E-mail address*: majc@st-andrews.ac.uk

[1]These primary authors contributed equally to this article

1. Introduction

Significant progress in understanding the mechanisms behind cancer development has been achieved in recent years by using molecular-based sequencing techniques (Bhang et al., 2015; Vermeulen et al., 2013; Wang et al., 2014; Ding et al., 2010; Zhang et al., 2014a; Yap et al., 2012; Martinez et al., 2013). Despite this growing knowledge, we are far from a complete understanding of the principles that govern the emergence of intratumour heterogeneity. This poses a major obstacle to successful cancer chemotherapy and management of disease relapse (Gerlinger et al., 2012; Marusyk et al., 2012; Pribluda et al., 2015).

A novel perspective on cancer therapeutics can be obtained from the accumulating evidence indicating that the progression of solid tumours is, in essence, an eco-evolutionary process (Merlo et al., 2006; Greaves and Maley, 2012; Pienta et al., 2008). Firstly, new phenotypic variants emerge in the tumour via mutations and epimutations. Afterwards, these variants are subject to natural selection, and they proliferate and die under the selective pressures of the tumour microenvironment. From this evolutionary viewpoint, spatial variations in the distribution of abiotic components of the tumour microenvironment (e.g. nutrients and therapeutic agents) may lead to the creation of distinct local niches and thus provide ecological opportunities for diversification (Alfarouk et al., 2013; Gillies et al., 2012; Meads et al., 2009; Trédan et al., 2007).

To explore *in silico* the validity of such an ecological argument linking heterogeneity in the distribution of abiotic components of the tumour microenvironment to the development and maintenance of phenotypic heterogeneity between cancer cells, we present here a space- and phenotype-structured model of selection dynamics in a solid tumour. Our model consists of an integro-differential equation (IDE) for the spatiotemporal evolution of the phenotypic distribution of cancer cells (Busse et al., 2016; Chisholm et al., 2015; Delitala and Lorenzi, 2012; Lavi et al., 2013; Lorenzi et al., 2016; Lorz et al., 2013; Perthame, 2006) coupled to a system of partial differential equations (PDEs) for the dynamics of abiotic factors (Macklin et al., 2009; Norris et al., 2006; Ward and King, 1997).

Recent studies based on various mathematical modelling approaches support related hypotheses concerning the emergence of intratumour hetero-

geneity. For instance, Fu et al. (2015) have proposed a model based on a multi-type stochastic branching process describing growth of cancer cells in multiple spatial compartments characterised by different environmental conditions. Further, Lorz et al. (2015) have developed an IDE model of phenotypic selection in a radially symmetric tumour spheroid viewed as a population structured by a phenotypic trait and a 1D spatial variable. More recently, Lloyd et al. (2016) have considered an evolutionary game theory model of habitat heterogeneity where the tumour is composed of two compartments – the tumour core and the tumour edge – treated as two different habitats. Although these studies provide a valuable proof of concept for the hypothesis that spatial gradients of abiotic factors cause the selection of different phenotypic properties in distinct regions within the same solid tumour, they are based on mathematical models that rely on rather strong simplifying modelling assumptions. In contrast to these, our mathematical model requires no specific assumptions on the tumour geometry, and its parameters can be linked to experimentally measurable quantities. For these reasons, the model presented here offers a more flexible and realistic mathematical framework for studying phenotypic selection between cancer cells within solid tumours.

In this paper, integrating the results of formal analyses with numerical simulations, we show that inhomogeneities in the spatial distribution of oxygen, which are currently observed in solid tumours, can promote the creation of distinct local niches and lead to the selection of different phenotypic variants within the same tumour. This process fosters the emergence of stable phenotypic heterogeneity and supports the presence of hypoxic cells resistant to cytotoxic therapy prior to treatment. Moreover, our theoretical results reveal how intratumour heterogeneity can reduce the efficacy of cytotoxic drugs, leading to poor treatment outcomes, and demonstrate the importance of integrating spatial data with ecological principles when evaluating the therapeutic response of solid tumours to cytotoxic therapy.

2. Model description

We identify the tumour geometry with a spatial domain $\Omega \subset \mathbb{R}^3$. At any time instant $t \geq 0$, we characterise the state of each cancer cell in the tumour by means of a pair $(\mathbf{x}, y) \in \Omega \times [0, 1]$. The vector $\mathbf{x} \in \Omega$ identifies the spatial position of the cell and the scalar variable $y \in [0, 1] \subset \mathbb{R}$ stands for the normalised expression level of a hypoxia-responsive gene (Chisholm et al., 2015;

Lorenzi et al., 2016; Lorz et al., 2013). Examples of hypoxia-responsive genes can be found, for instance, in (Strese et al., 2013; Zhao et al., 2013). Cells within the tumour proliferate and die due to competition for limited space. Moreover, a cytotoxic drug can be administered which acts by increasing the cell death rate. We assume increasing values of the phenotypic state y to be correlated with a progressive switch towards a hypoxic phenotype which, in turn, implies a progressive reduction in the proliferation rate (Gordan et al., 2007; Lloyd et al., 2016). Additionally, given that cytotoxic agents target mostly rapidly proliferating cells, we assume that higher values of the phenotypic state y correspond with higher levels of resistance to the cytotoxic drug (Brown and Giaccia, 1998; Durand and Raleigh, 1998).

We model the local population density of cells (i.e. the cell phenotypic distribution at position $\mathbf{x}$) at time t by means of the function $n(t, \mathbf{x}, y) \geq 0$. Given the local population density $n(t, \mathbf{x}, y)$, we define the local number density of cells $\rho(t, \mathbf{x})$ and the mean local phenotypic state of the cells $\mu(t, \mathbf{x})$ as follows

$$\rho(t, \mathbf{x}) = \int_0^1 n(t, \mathbf{x}, y)\, \mathrm{d}y \quad \text{and} \quad \mu(t, \mathbf{x}) = \frac{1}{\rho(t, \mathbf{x})} \int_0^1 y\, n(t, \mathbf{x}, y)\, \mathrm{d}y. \quad (2.1)$$

Finally, we introduce the functions $s(t, \mathbf{x}) \geq 0$ and $c(t, \mathbf{x}) \geq 0$ to model the local concentration of oxygen and cytotoxic drug at position $\mathbf{x}$ and time t, respectively.

2.1. Dynamics of cancer cells

The dynamics of the local population density $n(t, \mathbf{x}, y)$ is governed by the following nonlinear IDE

$$\frac{\partial n}{\partial t}(t, \mathbf{x}, y) = R\big(y, \rho(t, \mathbf{x}), s(t, \mathbf{x}), c(t, \mathbf{x})\big)\, n(t, \mathbf{x}, y). \quad (2.2)$$

In Eq. (2.2), the function $R\big(y, \rho(t, \mathbf{x}), s(t, \mathbf{x}), c(t, \mathbf{x})\big)$ represents the fitness of cells with phenotypic state y at position $\mathbf{x}$ and time t (i.e. the fitness landscape of the tumour), given the local environmental conditions determined by the local cell density $\rho(t, \mathbf{x})$ and the concentrations of abiotic factors $s(t, \mathbf{x})$ and $c(t, \mathbf{x})$. Throughout the paper, we define the fitness landscape of the tumour as

$$R\big(y, \rho(t, \mathbf{x}), s(t, \mathbf{x}), c(t, \mathbf{x})\big) = p(y, s(t, \mathbf{x})) - k(y, c(t, \mathbf{x})) - d\rho(t, \mathbf{x}). \quad (2.3)$$

The definition given by (2.3) relies on the idea that a higher cell density $\rho(t, \mathbf{x})$ at position $\mathbf{x}$ corresponds to a more intense competition for space. In particular, we let cells located at position $\mathbf{x}$ die with rate $d\rho(t, \mathbf{x})$, where the parameter $d > 0$ represents the death rate due to intratumour competition between cells. The function $k(y, c) \geq 0$ models the additional death rate due to the cytotoxic drug. Since increasing values of the phenotypic state y correspond to higher levels of cytotoxic-drug resistance, we assume the function k to be decreasing in the phenotypic state y. Moreover, since the death rate increases with higher drug concentrations, we assume the function k to be increasing in the drug dose c. The function $p(y, s) \geq 0$ represents the cell proliferation rate, which we define as

$$p(y, s(t, \mathbf{x})) = f(y) + r(y, s(t, \mathbf{x})). \tag{2.4}$$

The function $f(y)$ is the proliferation rate under hypoxic conditions and is, therefore, an increasing function of the phenotypic state y (Xia et al., 2014). The function $r(y, s)$ is decreasing in the phenotypic state y and increasing in the oxygen concentration s, since it models the rate of cell proliferation in oxygenated environments (Alfarouk et al., 2013). In this paper we consider

$$f(y) = \zeta \left[1 - (1 - y)^2\right], \tag{2.5}$$

$$r(y, s(t, \mathbf{x})) = \gamma_s \frac{s(t, \mathbf{x})}{\alpha_s + s(t, \mathbf{x})} \left(1 - y^2\right), \tag{2.6}$$

$$k(y, c(t, \mathbf{x})) = \gamma_c \frac{c(t, \mathbf{x})}{\alpha_c + c(t, \mathbf{x})} (1 - y)^2. \tag{2.7}$$

These definitions satisfy the generic properties listed above and ensure analytical tractability of the model. Furthermore, they lead naturally to a smooth fitness landscape which is close to the approximate fitness landscapes inferred from experimental data through regression techniques – see, for instance, (Otwinowski and Plotkin, 2014) and references therein. We note that when $y = 0$ the cells use purely aerobic respiration for proliferation and will not proliferate in the absence of oxygen. The state $y = 1$ denotes a purely hypoxic phenotype with a correspondingly reduced proliferation rate, which, however, is strictly positive (> 0) even in the absence of oxygen. The definitions given by (2.6) and (2.7) rely on the further assumption that the consumption of oxygen and the cytotoxic drug is governed by Michaelis-Menten kinetics with constants $\alpha_s > 0$ and $\alpha_c > 0$, respectively (Norris et al.,

2006; Ward and King, 1997). The parameter $\gamma_c > 0$ is the maximum cell death rate induced by the cytotoxic drug. The parameters $\zeta > 0$ and $\gamma_s > 0$ represent the maximum proliferation rate under hypoxic conditions and in oxygenated environments, respectively. Previous empirical studies suggest that cancer cells inhabiting hypoxic regions in solid tumours proliferate more slowly than cells populating oxygenated regions (Brown and Giaccia, 1998; Brown and Wilson, 2004; Lloyd et al., 2016). In our modelling framework, this observation is captured by the additional assumption $\zeta \ll \gamma_s$.

2.2. Dynamics of abiotic factors

The abiotic factors (i.e. oxygen and cytotoxic drug) diffuse in space, decay over time and are consumed by the cells. We note that the dynamics of abiotic factors is faster than cellular proliferation and death (Jacqueline et al., 2017; Walther et al., 2015). From a mathematical viewpoint, this means that we can assume oxygen and the cytotoxic drug to be in quasi-stationary equilibrium. In this setting, the dynamics of the functions $s(t, \mathbf{x})$ and $c(t, \mathbf{x})$ are described by the following elliptic PDEs which are coupled to the IDE (2.2)

$$\beta_s \Delta s(t, \mathbf{x}) = \eta_s \int_0^1 r\big(y, s(t, \mathbf{x})\big) n(t, \mathbf{x}, y)\, \mathrm{d}y \; + \; \lambda_s\, s(t, \mathbf{x}) \; + \; I_s(t, \mathbf{x}), \quad (2.8)$$

$$\beta_c \Delta c(t, \mathbf{x}) = \eta_c \int_0^1 k\big(y, c(t, \mathbf{x})\big) n(t, \mathbf{x}, y)\, \mathrm{d}y + \lambda_c\, c(t, \mathbf{x}) \; + \; I_c(t, \mathbf{x}). \quad (2.9)$$

In the above equations, the parameters $\beta_s > 0$ and $\beta_c > 0$ represent the diffusion constants of oxygen and the cytotoxic drug. The parameters $\eta_s > 0$ and $\eta_c > 0$ are scaling parameters for the consumption rate of abiotic factors by cells in the tumour. The parameters $\lambda_s > 0$ and $\lambda_c > 0$ represent the decay rates of oxygen and the cytotoxic drug. Finally, the terms $I_s(t, \mathbf{x})$ and $I_c(t, \mathbf{x})$ model sources and sinks of abiotic factors – one specific example we shall use in the sequel is a stationary (time-independent) influx of oxygen and cytotoxic drug into the tumour mass from blood vessels. Focussing on the biological scenario in which the concentrations of abiotic factors in the medium surrounding the tumour are constant in time, we make use of the following boundary conditions for (2.8) and (2.9)

$$s(\cdot, \mathbf{x}) = S(\mathbf{x}) \quad \text{and} \quad c(\cdot, \mathbf{x}) = C(\mathbf{x}), \quad \mathbf{x} \in \partial\Omega. \quad (2.10)$$

The functions $S(\mathbf{x})$ and $C(\mathbf{x})$ model the concentrations of oxygen and cytotoxic drug on the tumour boundary $\partial\Omega$.

3. Formal analysis of phenotypic selection

To obtain an analytical description of phenotypic selection, we assume that all possible phenotypic variants exist in the tumour at time $t = 0$, i.e. we set $n(0, \mathbf{x}, y) > 0$ for all $\mathbf{x} \in \Omega$ and all $y \in [0, 1]$. Additionally, we assume that the local cell density in the tumour is bounded above and below. In this scenario, for every position $\mathbf{x} \in \Omega$, the local cell density at equilibrium $\overline{\rho}(\mathbf{x})$ satisfies the following condition

$$\max_{y\in[0,1]} R\big(y, \overline{\rho}(\mathbf{x}), \overline{s}(\mathbf{x}), \overline{c}(\mathbf{x})\big) = 0,$$

where $\overline{s}(\mathbf{x})$ and $\overline{c}(\mathbf{x})$ stand for the steady-state distributions of oxygen and cytotoxic drug, respectively. Since the fitness landscape R is a monotonically decreasing function of the local number of cells, for every $\mathbf{x}$, there is a unique value of $\overline{\rho}(\mathbf{x})$ that satisfies the above relation. Moreover, given Eqs. (2.5)-(2.7), the fitness landscape R is a strictly concave function of y for all values of $\overline{\rho}(\mathbf{x})$, $\overline{s}(\mathbf{x})$ and $\overline{c}(\mathbf{x})$. This implies that, for all values of $\mathbf{x}$, there exists one single phenotypic state $\overline{y}(\mathbf{x})$ which maximises the fitness landscape R at equilibrium. Therefore, for each $\mathbf{x}$ there is a unique dominant phenotypic state $\overline{y}(\mathbf{x})$ (i.e. at each position $\mathbf{x}$ in the tumour, the equilibrium phenotypic distribution is unimodal). Given the phenotypic state $\overline{y}(\mathbf{x})$, the following conditions are simultaneously satisfied

$$R\big(\overline{y}(\mathbf{x}), \overline{\rho}(\mathbf{x}), \overline{s}(\mathbf{x}), \overline{c}(\mathbf{x})\big) = \max_{y\in[0,1]} R\big(y, \overline{\rho}(\mathbf{x}), \overline{s}(\mathbf{x}), \overline{c}(\mathbf{x})\big) = 0$$

and

$$\frac{\partial R}{\partial y}\big(\overline{y}(\mathbf{x}), \overline{\rho}(\mathbf{x}), \overline{s}(\mathbf{x}), \overline{c}(\mathbf{x})\big) = 0.$$

Together, the above considerations allow us to conclude that, given $\overline{s}(\mathbf{x})$ and $\overline{c}(\mathbf{x})$, there exists a unique pair $(\overline{\rho}(\mathbf{x}), \overline{y}(\mathbf{x}))$ which solves the following system of equations

$$\begin{cases} R\big(\overline{y}(\mathbf{x}), \overline{\rho}(\mathbf{x}), \overline{s}(\mathbf{x}), \overline{c}(\mathbf{x})\big) = 0, \\ \\ \dfrac{\partial R}{\partial y}\big(\overline{y}(\mathbf{x}), \overline{\rho}(\mathbf{x}), \overline{s}(\mathbf{x}), \overline{c}(\mathbf{x})\big) = 0. \end{cases} \tag{3.1}$$

For every position $\mathbf{x} \in \Omega$, the pair $\big(\overline{\rho}(\mathbf{x}), \overline{y}(\mathbf{x})\big)$ characterises the local cell density and the dominant phenotypic state at equilibrium. The formal arguments presented above are consistent with the asymptotic analysis developed

by Mirrahimi and Perthame (2015) for a system of equations modelling selection dynamics in a population structured by a phenotypic trait and a 1D spatial variable.

Solving the system of equations (3.1) we obtain

$$\overline{\rho}(\mathbf{x}) = \frac{1}{d}\left[A_{\overline{s}}(\mathbf{x}) - A_{\overline{c}}(\mathbf{x}) + \frac{\left(\zeta + A_{\overline{c}}(\mathbf{x})\right)^2}{\zeta + A_{\overline{s}}(\mathbf{x}) + A_{\overline{c}}(\mathbf{x})}\right] \tag{3.2}$$

and

$$\overline{y}(\mathbf{x}) = \frac{\zeta + A_{\overline{c}}(\mathbf{x})}{\zeta + A_{\overline{s}}(\mathbf{x}) + A_{\overline{c}}(\mathbf{x})}, \tag{3.3}$$

where

$$A_{\overline{s}}(\mathbf{x}) = \gamma_s \frac{\overline{s}(\mathbf{x})}{\alpha_s + \overline{s}(\mathbf{x})} \quad \text{and} \quad A_{\overline{c}}(\mathbf{x}) = \gamma_c \frac{\overline{c}(\mathbf{x})}{\alpha_c + \overline{c}(\mathbf{x})}.$$

Here, the expressions given by equations (3.2) and (3.3) demonstrate that the local cell density $\overline{\rho}$ and the phenotypic state $\overline{y}$ that maximises the cellular fitness at position $\mathbf{x}$ are determined by the concentrations of oxygen $\overline{s}$ and cytotoxic drug $\overline{c}$ at the same position. This is illustrated by the heat maps in Fig. 1, which show how, for the parameter values listed in Table 1, the values of $\overline{\rho}$ and $\overline{y}$ vary as functions of $\overline{s}$ and $\overline{c}$.

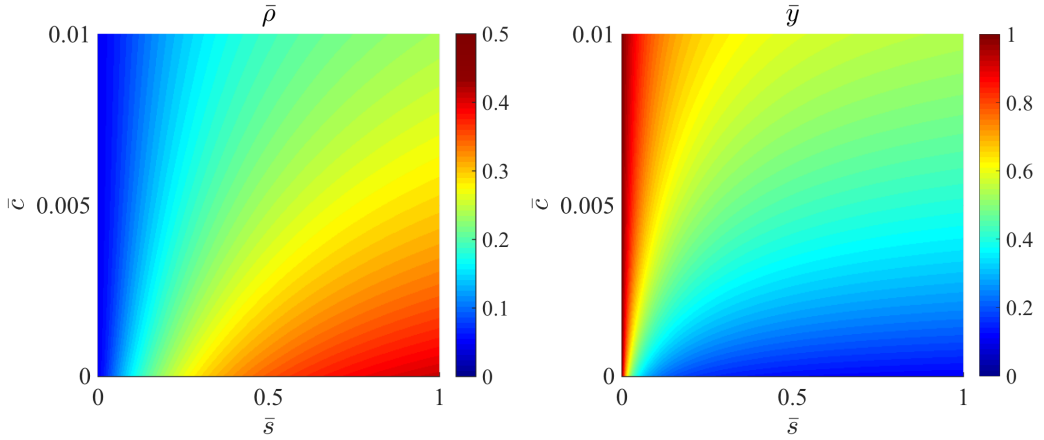

Figure 1: *Plots of the local cell density $\overline{\rho}$ and the dominant phenotypic state $\overline{y}$ at equilibrium as a function of the local concentration of oxygen $\overline{s}$ and cytotoxic drug $\overline{c}$. The quantities $\overline{\rho}$, $\overline{s}$ and $\overline{c}$ are scaled by the reference values ρ_0, s_0 and c_0 given in Table 1.*

Together, these results suggest that local variations of abiotic factors in the tumour microenvironment determine spatial variations of the selected phenotypic variants and cell densities. Specifically, lower values of the oxygen concentration $\overline{s}$ and higher values of the drug concentration $\overline{c}$ correspond to higher values of the phenotypic state $\overline{y}$ and lower values of the local cell density $\overline{\rho}$. Biologically, this means that local environments hostile to highly proliferative cells (i.e. environments characterised by lower oxygen availability and higher concentration of the cytotoxic agent) promote the selection of cells characterised by higher levels of expression of the hypoxia-responsive gene, which in turn leads to smaller cell numbers. On the contrary, higher values of $\overline{s}$ and lower values of $\overline{c}$ correspond to lower values of $\overline{y}$ and higher values of $\overline{\rho}$. Biologically, this means that highly proliferative cells are selected for in regions with higher oxygen and lower drug concentration, which in turn leads to larger cell densities.

Table 1: *Parameter values used to perform numerical simulations. Further details about the model parameters can be found in Appendix A.*

Parameter	Biological meaning	Value
α_c	Michaelis-Menten constant of cytotoxic drug	$2 \times 10^{-6}\ g\,cm^{-3}$
α_s	Michaelis-Menten constant of oxygen	$1.5 \times 10^{-7}\ g\,cm^{-3}$
β_c	Diffusion coefficient of cytotoxic drug	$5 \times 10^{-6}\ cm^2\,s^{-1}$
β_s	Diffusion coefficient of oxygen	$2 \times 10^{-5}\ cm^2\,s^{-1}$
γ_c	Maximum cell death rate induced by cytotoxic drug	$1.8 \times 10^{-4}\ s^{-1}$
γ_s	Maximum cell proliferation rate in oxygenated environments	$1 \times 10^{-5}\ s^{-1}$
ζ	Maximum cell proliferation rate under hypoxic conditions	$1 \times 10^{-6}\ s^{-1}$
d	Rate of cell death due to competition for space	$2 \times 10^{-14}\ cm^3\,s^{-1}\,cell^{-1}$
η_c	Scaling factor for cell consumption of cytotoxic drug	$4 \times 10^{-12}\ g\,cell^{-1}$
η_s	Scaling factor for cell consumption of oxygen	$2 \times 10^{-12}\ g\,cell^{-1}$
λ_c	Decay rate of cytotoxic drug	$0.1\ s^{-1}$
λ_s	Decay rate of oxygen	$0.3\ s^{-1}$
ρ_0	Reference value for the local cell density	$10^9\ cells\,cm^{-3}$
s_0	Reference value for the local concentration of oxygen	$6.3996 \times 10^{-7}\ g\,cm^{-3}$
c_0	Reference value for the local concentration of cytotoxic drug	$10^{-5}\ g\,cm^{-3}$

4. Numerical solutions

We combine the formal results established in the previous section with numerical simulations of the coupled system given by Eqs. (2.2), (2.8) and (2.9). We consider both the case where the spatial domain Ω is an *in silico* tumour spheroid as well as the case in which the domain Ω corresponds to the three dimensional geometry of an actual *in vivo* human hepatic tumour. The hepatic tumour was imaged using 3D computerised tomography

and the image data has been obtained from the 3D-IRCADb-01 database (http://www.ircad.fr/).

For the numerical simulations, we use the parameter values from the existing literature which are listed in Table 1. Further details of the model parametrisation are given in Appendix A, whilst a complete description of the numerical methods used in this work can be found in Appendix B. Firstly, we report here on results obtained under the assumption that the tumour is avascular (i.e. $I_s(t, \mathbf{x}) = 0$ and $I_c(t, \mathbf{x}) = 0$ for all $t \geq 0$ and $\mathbf{x} \in \Omega$) and the concentrations of oxygen and cytotoxic drug on the boundary $\partial\Omega$ are constant (i.e. $S(\mathbf{x}) = s_0$ and $C(\mathbf{x}) = c_0$ for all $\mathbf{x} \in \partial\Omega$). Secondly, we carry out numerical simulations in the case where oxygen and the cytotoxic drug are brought into the tumour from blood vessels which are enclosed within the tumour mass. The results obtained are presented and discussed at the end of this section. In the latter case, we define Ω_v to be the region inside the tumour in which the blood vessels are present and set $I_s(\cdot, \mathbf{x}) = s_0$ and $I_c(\cdot, \mathbf{x}) = c_0$ for $\mathbf{x} \in \Omega_v$ and $I_s(\cdot, \mathbf{x}) = I_c(\cdot, \mathbf{x}) = 0$ for $\mathbf{x} \in \Omega \setminus \Omega_v$. Similarly we set $S(\mathbf{x}) = s_0$ and $C(\mathbf{x}) = c_0$ for $\mathbf{x} \in \partial\Omega_v$ and $S(\mathbf{x}) = C(\mathbf{x}) = 0$ for $\mathbf{x} \in \partial\Omega \setminus \partial\Omega_v$.

4.1. In silico tumour spheroid simulations

The results obtained with and without the cytotoxic drug are presented in Fig. 2, where the local concentrations of abiotic factors, the local mean phenotypic state and the local cell density at equilibrium are shown.

The concentrations of oxygen and cytotoxic drug, when present, decrease monotonically from the edge to the centre of the spheroid. As a consequence, in the absence of drug (plots in the top row of Fig. 2), the local cell density decays radially with maximum value on the spheroid boundary. We observe the formation of a necrotic core, with very few living cells, surrounded by a hypoxic region, then by a more densely populated rim with more living cells present. Biologically, our results suggest that the outer part of the spheroid becomes colonised by highly proliferative cells, while slow-proliferating cells with a hypoxic phenotype are selected for in the interior of the spheroid. Accordingly, the local mean phenotypic state is a radially decreasing function from the centre to the boundary of the spheroid.

When the cytotoxic drug is present (plots in the bottom row of Fig. 2), the number of living cells is consistently reduced throughout the whole tumour spheroid. The selective pressure exerted by the drug drives the mean phenotypic state towards drug-resistance. Moreover, the local cell density

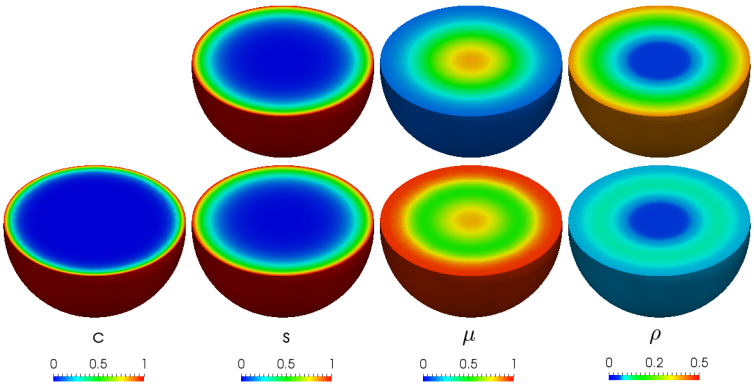

Figure 2: *Plots of the local concentration of cytotoxic drug $c(t, \mathbf{x})$, the local concentration of oxygen $s(t, \mathbf{x})$, the local mean phenotypic state $\mu(t, \mathbf{x})$ and the local cell density $\rho(t, \mathbf{x})$ at $t = 70$ days [i.e. close to the steady state of Eqs. (2.2), (2.8) and (2.9)] in an in silico tumour spheroid of radius $800\mu m$. The top and bottom rows refer to the cases when the cytotoxic drug is absent and present, respectively. For better visualisation, only the bottom half of the spheroid is shown. The quantities c, s and ρ are scaled by the reference values c_0, s_0 and ρ_0 given in Table 1.*

and the local mean phenotypic state are no longer monotonic functions of the distance from the centre of the spheroid. In this case, the density of living cells is close to zero at both the boundary and the core of the tumour. Therefore, most of the surviving cells are found in a thin band in the interior of the spheroid where the local mean phenotypic state attains its minimum.

Both with and without the cytotoxic drug, at each position $\mathbf{x}$ the phenotypic distribution $n(t, \mathbf{x}, y)$ has a Gaussian-like profile (see Fig. S1 in the supplementary material); therefore, the local mean phenotypic state coincides with the locally dominant phenotypic state. To this end, Movie S1 in the supplementary material demonstrates that after a short time period of transient behaviour, the local cell density $\rho(t, \mathbf{x})$ and the local mean phenotypic state $\mu(t, \mathbf{x})$ converge, respectively, to the equilibrium values of the local cell density $\overline{\rho}(\mathbf{x})$, given by Eq. (3.2), and of the dominant phenotypic state $\overline{y}(\mathbf{x})$, given by Eq. (3.3).

4.2. In vivo human hepatic tumour simulations

Figure 3 shows the computerised tomography scan of an actual human liver tumour which we selected as the spatial domain Ω (obtained from the 3D-IRCADb-01 database which can be found at URL http://www.ircad.fr/).

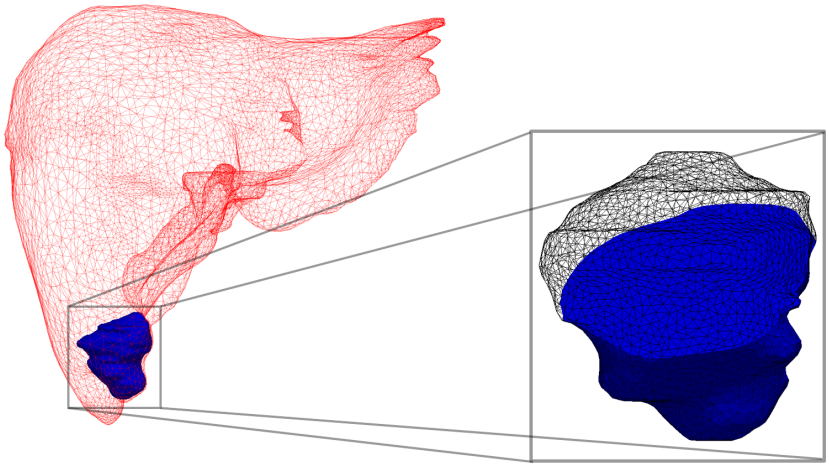

Figure 3: *Computerised tomography scan of a human tumour (blue) shown in situ within the liver (red). The maximum diameter of the tumour is approximatively* $3200\mu m$*. The inset shows a magnification of the tumour with a portion made transparent, as in Fig. 4, in order to visualise the tumour bulk.*

Our numerical simulations indicate that the spatial distributions of cells, oxygen and cytotoxic drug as well as the spatial patterns of phenotypic selection for the hepatic tumour are qualitatively similar to those observed in the *in silico* tumour spheroid (compare the results in Fig. 4 with the results of Fig. 2, and the results of Movie S1 with the results displayed by Movie S2 in the supplementary material).

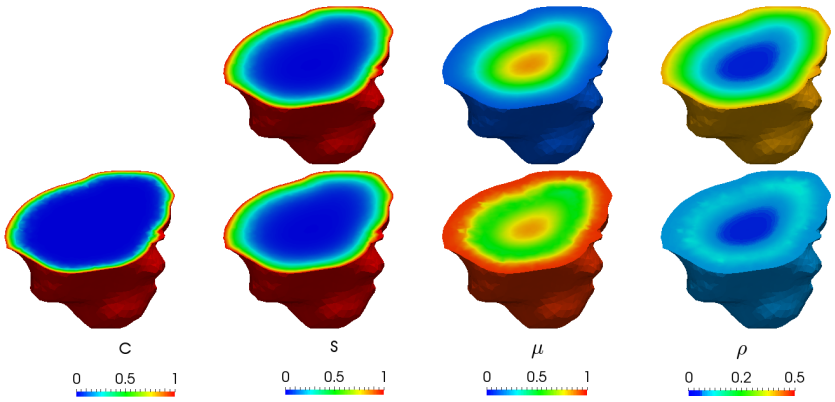

Figure 4: *Plots of the local concentration of cytotoxic drug $c(t, \mathbf{x})$, the local concentration of oxygen $s(t, \mathbf{x})$, the local mean phenotypic state $\mu(t, \mathbf{x})$ and the local cell density $\rho(t, \mathbf{x})$ at $t = 70$ days [i.e. close to the steady state of Eqs. (2.2), (2.8) and (2.9)] in the human hepatic tumour of Fig. 3. The top and bottom row refer to the cases when the cytotoxic drug is absent and present, respectively. For better visualisation, only a portion of the tumour is shown. The quantities c, s and ρ are scaled by the reference values c_0, s_0 and ρ_0 given in Table 1.*

4.3. Effects of tumour vasculature

In order to investigate the effects of tumour vasculature on phenotypic selection, we included some artificial blood vessels into the tumour mass of Fig. 3. In particular, we focused on the case in which the spatial domain Ω is given by the tumour mass shown in Fig. 5.

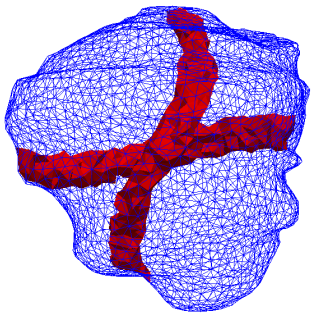

Figure 5: *Human hepatic tumour of Fig. 3 with the addition of artificial blood vessels.*

The results shown in Fig. 6 and Movie S3 in the supplementary material indicate that conclusions similar to those achieved in the previous sections apply to the case with tumour vasculature. Specifically, when the cytotoxic

drug is not present, highly proliferative cells are selected for in the tumour areas where oxygen concentration is higher. Conversely, poorly oxygenated regions are colonised by slow-proliferating cells which express hypoxic phenotypes. These hypoxic cells, characterised by lower levels of drug-sensitivity, become dominant within the tumour upon delivery of the cytotoxic drug.

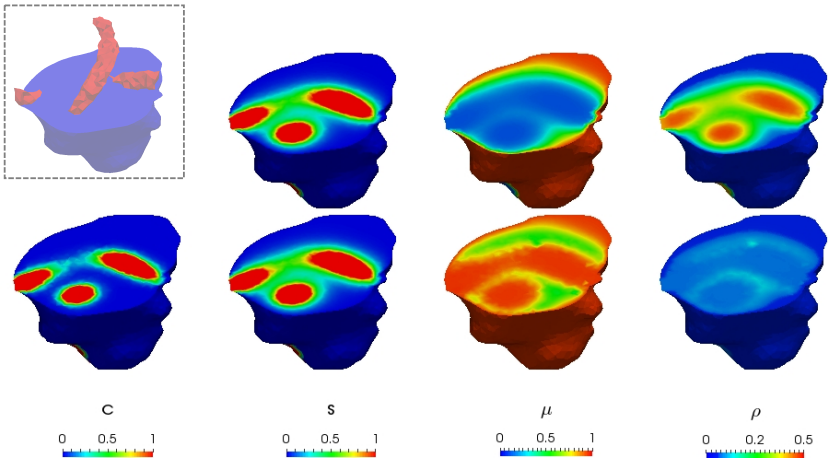

Figure 6: *Plots of the local concentration of cytotoxic drug $c(t, \mathbf{x})$, the local concentration of oxygen $s(t, \mathbf{x})$, the local mean phenotypic state $\mu(t, \mathbf{x})$ and the local cell density $\rho(t, \mathbf{x})$ at $t = 70$ days [i.e. close to the steady state of Eqs. (2.2), (2.8) and (2.9)] in the human hepatic tumour with vasculature of Fig. 5. For better visualisation, only the bottom half of the tumour is shown as in the inset. The top and bottom row display the results obtained in the absence and in the presence of cytotoxic drug, respectively. The quantities c, s and ρ are scaled by the reference values c_0, s_0 and ρ_0 given in Table 1.*

5. Discussion and conclusions

Our analysis and numerical simulations support the hypothesis that spatial variations in oxygen levels can foster the emergence of phenotypic heterogeneity by promoting the creation of distinct local niches within the same tumour. Our model predicts that well-oxygenated regions of the tumour will be densely populated by highly proliferative cancer cells characterised by higher oxygen uptake. Conversely, hypoxic cells with lower proliferation rates colonise tumour regions hostile to fast-proliferating cells – such as the regions of the tumour where oxygen concentration is lower.

Our modelling framework offers a plausible theoretical basis for recent experimental results suggesting that the periphery and the centre of avascu-

lar tumours represent distinct ecological niches (Brown and Giaccia, 1998; Hoefflin et al., 2016; Lloyd et al., 2016; Tannock, 1968; Zhang et al., 2014b). Furthermore, our findings agree with observations made in mathematical modelling and experimental studies (Adamski et al., 2013; Brown and Giaccia, 1998; Powathil et al., 2012; Sullivan et al., 2008; Wartenberg et al., 2003) which suggest that hypoxia favours the selection for cancer cells resistant to cytotoxic therapy prior to treatment. Consequently, this facilitates the development of resistance following drug exposure.

Our analysis and numerical simulations also address the open question of how phenotypic heterogeneity in a solid tumour changes under cytotoxic therapy. Our results complement those of Robertson-Tessi et al. (2015) by demonstrating that cytotoxic agents decrease the number of living cancer cells and select for more resistant phenotypic variants throughout the whole tumour. In particular, since cytotoxic drugs kill more proliferative cells in regions of the tumour with higher oxygen concentration, the drug exposure removes the selective barrier limiting the growth of less proliferative and more resistant cells. This reduces drug efficacy, and ultimately leads to poor treatment outcomes and low patient survival rates (Sottoriva et al., 2013; Williams et al., 2016; Jones et al., 2008).

In summary, our mathematical study highlights the role that the spatial distribution of abiotic components in the tumour microenvironment play in mediating phenotypic heterogeneity in solid tumours. Our results strongly support the need for spatial data when performing phenotypic profiling of solid tumours, as single tumour biopsies are unlikely to fully represent the complete phenotypic landscape of the tumour (Ding et al., 2010; Zhang et al., 2014a; Yap et al., 2012; Martinez et al., 2013; Schwarz et al., 2015).

Histological analyses indicate that solid tumours contain cancer cells with a wide spectrum of gene expression. However, our theoretical work provides support for the ideas proposed by Alfarouk et al. (2013), who have noted that the phenotypes of cancer cells result, to an extent, from predictable spatial gradients in the concentrations of abiotic factors which can be mapped out via non-invasive imaging techniques (Beerenwinkel et al., 2016). Under this perspective, knowing how abiotic factors shape the phenotypic characteristics of cancer cells, spatial patterns of tumour perfusion reconstructed from clinical cancer images could be used to inform molecularly targeted therapy combinations (Lopez and Banerji, 2016). This may open up new avenues of research for exploiting ecological principles to design innovative therapeutic protocols along the lines of adaptive therapy (Gatenby et al., 2009; Ibrahim-

Hashim et al., 2017).

Additional strengths of the present study are that the parameter values used to perform numerical simulations come from existing literature, and the outcomes of our formal analysis are characterised by broad structural stability under parameter changes. Our framework can accommodate parameter values for any solid tumour and the method we have used to construct numerical solutions of the model is applicable to arbitrary geometries. Therefore, while we performed numerical simulations on the geometry of a given *in vivo* human hepatic tumour as an illustrative example, our *in silico* approach can be applied to studying phenotypic selection between cancer cells in a wide range of neoplasms.

Finally, while we have assumed multiple phenotypic variants to be present in the tumour from the beginning of simulations and we have considered the tumour size to remain constant over time, the modelling framework presented here can be extended to incorporate mutations and epimutations (Chisholm et al., 2015; Lorenzi et al., 2016) as well as growing tumour spatial domains (Ambrosi and Preziosi, 2002; Byrne and Chaplain, 1996; Byrne and Drasdo, 2009; Lorenzi et al., 2017; Perthame et al., 2014; Tang et al., 2013). Given the robustness and structural stability of our results, we expect the main conclusions of this work to hold even after the inclusion of these additional layers of biological complexity.

Acknowledgments

The authors would like to thank Dana-Adriana Botesteanu for her helpful feedback and insightful comments and suggestions. CV wishes to acknowledge partial support from the European Union's Horizon 2020 research and innovation programme under the Marie Sklodowska-Curie grant agreement No 642866. AL was supported by King Abdullah University of Science and Technology (KAUST) baseline and start-up funds (BAS/1/1648-01-01 and BAS/1/1648-01-02). MAJC gratefully acknowledge support of EPSRC grant no. EP/N014642/1.

A. Model parametrisation

A.1. Dynamics of oxygen

In agreement with the considerations made by Ward and King (1997) and the experimental results reported by Casciari et al. (1992), we set the Michaelis-Menten constant of oxygen $\alpha_s = 1.5 \times 10^{-7}\ g\,cm^{-3}$, the maximum cell proliferation rate in oxygenated environments $\gamma_s = 1 \times 10^{-5}\ s^{-1}$ and the conversion factor for cell consumption of oxygen $\eta_s = 2 \times 10^{-12}\ g\,cell^{-1}$. Moreover, following Ward and King (1997), we make reference to the experimental results by Hlatky and Alpen (1985) and set the diffusion coefficient of oxygen $\beta_s = 2 \times 10^{-5}\ cm^2\,s^{-1}$. Also, we choose the natural decay rate of oxygen $\lambda_s = 0.3\ s^{-1}$ in order to be consistent with the parameter values used by Macklin et al. (2009).

A.2. Dynamics of cells

We set the rate of cell death due to competition for space $d = 2 \times 10^{-14}\ cm^3\,s^{-1}\,cell^{-1}$ so that the equilibrium value of the local cell density $\overline{\rho}$ in the presence of high oxygen concentrations (i.e. for $\frac{\overline{s}}{\alpha_s+\overline{s}} \approx 1$) is approximatively $5 \times 10^8\ cell\,cm^{-3}$, which is consistent with the experimental values reported in (Li, 1982). Moreover, in agreement with experimental results on cell proliferation presented in (Gordan et al., 2007), we choose the maximum proliferation rate of cells under hypoxic conditions ζ to be one order of magnitude smaller than γ_s.

A.3. Dynamics of the cytotoxic drug

In agreement with the considerations made by Norris et al. (2006) and the experimental results reported by Kwok and Twentyman (1985), we set the Michaelis-Menten constant of the cytotoxic drug $\alpha_c = 2 \times 10^{-6}\ g\,cm^{-3}$, the maximum rate of cell death induced by the cytotoxic drug $\gamma_c = 1.8 \times 10^{-4}\ s^{-1}$ and the conversion factor for cell consumption of the cytotoxic drug $\eta_c = 4 \times 10^{-12}\ g\,cell^{-1}$. The diffusion coefficients of cytotoxic drugs vary depending on the size of the molecules and the permeability of the surrounding tissue (Norris et al., 2006). In order to be consistent with the experimental results reported in (Levin et al., 1980), we the set diffusion coefficient of the cytotoxic drug $\beta_c = 5 \times 10^{-6}\ cm^2\,s^{-1}$. Furthermore, we choose the natural decay rate of the cytotoxic drug $\lambda_c = 0.1\ s^{-1}$ based on the biological data reported in (Calabresi et al., 1985).

A.4. Reference quantities t_0, x_0, ρ_0, s_0 and c_0

We set $t_0 = 1\ s$, $x_0 = 10^{-3}\ cm$ [which corresponds to typical values of cell radii (Melicow, 1982)], $\rho_0 = 10^9\ cells\, cm^{-3}$ [which is consistent with experimental measurements of cell densities in solid tumours (Li, 1982)], $s_0 = 6.3996 \times 10^{-7}\ g\, cm^{-3}$ [which is consistent with experimental data on oxygen concentrations reported in (Kumosa et al., 2014)] and $c_0 = 10^{-5}\ g\, cm^{-3}$ [which corresponds to values for cytotoxic drug concentrations used in (Norris et al., 2006)].

B. Numerical methods and further details of numerical simulations

The integro-differential equation for $n(t, \mathbf{x}, y)$ is approximated using a semi-implicit Euler method, whilst the system of elliptic partial differential equations for $s(t, \mathbf{x})$ and $c(t, \mathbf{x})$ is approximated using a finite element method with linear basis functions. To this end, we construct a triangulation $\mathcal{T}$ of the spatial domain Ω, which divides Ω into a finite number of non-degenerate and non-overlapping tetrahedra such that the triangulation contains no hanging nodes. We denote by $\mathbb{V}$ the space of all continuous piecewise linear functions on $\mathcal{T}$. Let N_t and N_y be positive integers, we define the uniform (for simplicity) time-step $\tau = T/N_t$, with T being the end time of simulations, and trait-step $h_y = 1/N_y$. For each $l \in \{0, 1, \ldots, N_t\}$ and each $j \in \{0, 1, \ldots, N_y\}$ we define $t^l := l\tau$ and $y_j := jh_y$.

Let $\{\mathbf{x}_i\}_{i=0,\ldots,N_h}$ denote the set of vertices of the triangulation $\mathcal{T}$. We look for approximations to the oxygen and cytotoxic drug concentrations, that is, $s_h^l := s_h(t^l) \in \mathbb{V}$ and $c_h^l := c_h(t^l) \in \mathbb{V}$ with $l = 0, \ldots, N_t$, and for the density of cells in the phenotypic state y_j, that is, $(n_h)_j^l := n_h(t^l, y_j) \in \mathbb{V}$ with $l = 0, \ldots, N_t$ and $j = 0, \ldots, N_y$.

We define our nodal approximations as $n_{i,j}^l := n_h(t^l, \mathbf{x}_i, y_j)$, $s_i^l := s_h(t^l, \mathbf{x}_i)$ and $c_i^l := c_h(t^l, \mathbf{x}_i)$. One step of our numerical scheme is as follows: given $\left\{(n_h)_j^{l-1}\right\}_{j=0,\ldots,N_y}$, $s_h^{l-1}, c_h^{l-1} \in \mathbb{V}$, find $\left\{(n_h)_j^l\right\}_{j=0,\ldots,N_y}, s_h^l, c_h^l \in \mathbb{V}$ such that, for $i = 0, \ldots, N_h$ and $j = 0, \ldots, N_y$,

$$n_{i,j}^l = n_{i,j}^{l-1}\left\{1 - \tau\left[p\left(y_j, s_i^{l-1}\right) - k\left(y_j, c_i^{l-1}\right) - \frac{d}{N_y + 1}\sum_{k=0}^{N_y} n_{i,k}^{l-1}\right]\right\}^{-1},$$

and for all $\Phi \in \mathbb{V}$,

$$\int_\Omega \left(\beta_s \nabla s_h^l \nabla \Phi - \lambda_s s_h^l \Phi\right) \mathrm{d}\mathbf{x} = \int_\Omega \left[\frac{1}{N_y + 1}\left(\sum_{k=0}^{N_y} r\left(y_k, s_h^{l-1}\right)(n_h)_j^l\right) + I_s^l\right] \Phi \mathrm{d}\mathbf{x}$$

and

$$\int_{\Omega}\left(\beta_c\nabla c_h^l\nabla\Phi-\lambda_c c_h^l\Phi\right)\mathrm{d}\mathbf{x}=\int_{\Omega}\left[\frac{1}{N_y+1}\left(\sum_{k=0}^{N_y}k\left(y_k,c_h^{l-1}\right)\left(n_h\right)_k^l\right)+I_c^l\right]\Phi\mathrm{d}\mathbf{x}.$$

The explicit treatment of the nonlinear terms leads to the equations being decoupled, so that only linear systems must be solved at each time-step. We have investigated both Picard linearisation and Newton linearisation; the results remain qualitatively unchanged. Our implementation makes use of the ALBERTA C finite element toolbox Schmidt and Siebert (2005).

For all the simulations we report on in this work, we took the initial local population density $n(t=0,\mathbf{x},y)$ to be uniform in $\mathbf{x}$ and a weighted Gaussian in y with local average phenotype $\mu(t=0,\mathbf{x})=0.5$ for all $\mathbf{x}\in\Omega$. The initial local cell density was $\rho(t=0,\mathbf{x})=5\times10^8\ cells\,cm^{-3}$ for any $\mathbf{x}\in\Omega$. We verified through additional numerical simulations that, as one would expect, the long-time behaviour of $n(t,\mathbf{x},y)$ does not depend on the choice of the initial condition. In the absence of blood vessels, we set $I_s(t,\mathbf{x})=0$ and $I_c(t,\mathbf{x})=0$ for all $t\geq0$ and $x\in\Omega$, and we used the boundary conditions $S(\mathbf{x})=s_0$ and $C(\mathbf{x})=c_0$ for all $x\in\partial\Omega$. In the presence of blood vessels (vid. Fig. 5), we set $I_s(t,\mathbf{x})=s_0$ and $I_c(t,\mathbf{x})=c_0$ in the blood vessels and $I_s(t,\mathbf{x})=I_c(t,\mathbf{x})=0$ otherwise, and similarly we used the boundary conditions $S(\mathbf{x})=s_0$ and $C(\mathbf{x})=c_0$ at points where the blood vessels meet the tumour boundary and $S(\mathbf{x})=C(\mathbf{x})=0$ at all other points on the boundary.

For the purpose of robust simulations, we non-dimensionalised the governing equations of the model as described in Appendix C. We used non-dimensional parameters corresponding to the dimensional values provided in Table 1 and discussed in Appendix A. To compute numerical solutions, we used a time-step corresponding to $\tau=2\times10^3\,s$ and select $t_f=10^7\,s$ as the end time; furthermore, we chose $N_y=50$, giving a phenotypic-step $h_y=0.02$. We verified that the results remain qualitatively unchanged for one level of refinement of all the discretisation parameters. To carry out numerical simulations, we used a mesh consisting of 393216 tetrahedra with 68705 degrees of freedom for the multicellular tumour spheroid and a mesh consisting 53292 tetrahedra with 9932 degrees of freedom for the hepatic tumour. The meshing software CGAL (http://www.cgal.org) was used to construct a tetrahedral mesh of the tumour.

C. Non-dimensionalisation of the model

Denoting dimensionless variables by carets, we adopt the following rescalings:

$$\hat{t} = \frac{t}{t_0}, \quad \hat{\mathbf{x}} = \frac{\mathbf{x}}{x_0},$$

$$\hat{n}(\hat{t}, \hat{\mathbf{x}}, y) = \frac{n(t, \mathbf{x}, y)}{\rho_0}\,, \quad \hat{s}(\hat{t}, \hat{\mathbf{x}}) = \frac{s(t, \mathbf{x})}{s_0}, \quad \hat{c}(\hat{t}, \hat{\mathbf{x}}) = \frac{c(t, \mathbf{x})}{c_0},$$

$$\hat{\alpha}_s = \frac{\alpha_s}{s_0}, \quad \hat{\alpha}_c = \frac{\alpha_c}{c_0}, \quad \hat{\gamma}_s = t_0\,\gamma_s, \quad \hat{\gamma}_c = t_0\,\gamma_c \quad \hat{\zeta} = t_0\,\zeta, \quad \hat{d} = t_0\,d\,\rho_0,$$

$$\hat{\beta}_s = \frac{t_0\,\beta_s}{r_0^2}, \quad \hat{\beta}_c = \frac{t_0\,\beta_c}{r_0^2}, \quad \hat{\eta}_s = \frac{\eta_s}{s_0}\rho_0 \quad \hat{\eta}_c = \frac{\eta_c}{c_0}\rho_0, \quad \hat{\lambda}_s = t_0\,\lambda_s \quad \hat{\lambda}_c = t_0\,\lambda_c$$

and

$$\hat{I}_s(\hat{t}, \hat{\mathbf{x}}) = t_0 \frac{I_s(t, \mathbf{x})}{s_0}, \qquad \hat{I}_c(\hat{t}, \hat{\mathbf{x}}) = t_0 \frac{I_c(t, \mathbf{x})}{c_0}.$$

Here, t_0, x_0, ρ_0, s_0 and c_0 denote suitable reference values (vid. Appendix A). Under these rescalings, the governing equations of our model become:

$$\frac{\partial \hat{n}}{\partial \hat{t}}(\hat{t}, \hat{\mathbf{x}}, y) = \hat{R}\big(y, \hat{\rho}(\hat{t}, \hat{\mathbf{x}}), \hat{s}(\hat{t}, \hat{\mathbf{x}}), \hat{c}(\hat{t}, \hat{\mathbf{x}})\big)\; \hat{n}(\hat{t}, \hat{\mathbf{x}}, y), \quad (\hat{\mathbf{x}}, y) \in \hat{\Omega} \times [0, 1],$$

$$\hat{R}\big(y, \hat{\rho}, \hat{s}, \hat{c}\big) := \hat{\zeta}\,\Big[1 - (1-y)^2\Big] + \hat{\gamma_s}\,\frac{\hat{s}}{\hat{\alpha}_s + \hat{s}}\,\big(1 - y^2\big) - \hat{\gamma_c}\,\frac{\hat{c}}{\hat{\alpha}_c + \hat{c}}\,(1-y)^2 - \hat{d}\,\hat{\rho},$$

$$\hat{\beta}_s\,\Delta\hat{s}(\hat{t}, \hat{\mathbf{x}}) = \hat{\eta}_s\,\hat{\gamma}_s\,\frac{\hat{s}(\hat{t}, \hat{\mathbf{x}})}{\hat{\alpha}_s + \hat{s}(\hat{t}, \hat{\mathbf{x}})}\,\int_0^1 \big(1 - y^2\big)\,\hat{n}(\hat{t}, \hat{\mathbf{x}}, y)\,dy + \hat{\lambda}_s\,\hat{s} + \hat{I}_s(\hat{t}, \hat{\mathbf{x}}),$$

$$\hat{\beta}_c\,\Delta\hat{c}(\hat{t}, \hat{\mathbf{x}}) = \hat{\eta}_c\,\hat{\gamma}_c\,\frac{\hat{c}(\hat{t}, \hat{\mathbf{x}})}{\hat{\alpha}_c + \hat{c}(\hat{t}, \hat{\mathbf{x}})}\,\int_0^1 (1 - y)^2\,\hat{n}(\hat{t}, \hat{\mathbf{x}}, y)\,dy + \hat{\lambda}_c\,\hat{c} + \hat{I}_c(\hat{t}, \hat{\mathbf{x}}).$$

References

Adamski, J., Price, A., Dive, C., Makin, G., 2013. Hypoxia–induced cytotoxic drug resistance in osteosarcoma is independent of hif-1alpha. PloS One 8 (6), e65304.

Alfarouk, K. O., Ibrahim, M. E., Gatenby, R. A., Brown, J. S., 2013. Riparian ecosystems in human cancers. Evolutionary Applications 6 (1), 46–53.

Ambrosi, D., Preziosi, L., 2002. On the closure of mass balance models for tumor growth. Mathematical Models and Methods in Applied Sciences 12 (05), 737–754.

Beerenwinkel, N., Greenman, C. D., Lagergren, J., 2016. Computational cancer biology: an evolutionary perspective. PLoS Computational Biology 12 (2), e1004717.

Bhang, H. C., Ruddy, D. A., Radhakrishna, V. K., Caushi, J. X., Zhao, R., Hims, M. M., Singh, A. P., Kao, I., Rakiec, D., Shaw, P., et al., 2015. Studying clonal dynamics in response to cancer therapy using high-complexity barcoding. Nature medicine 21 (5), 440–448.

Brown, J. M., Giaccia, A. J., 1998. The unique physiology of solid tumors: opportunities (and problems) for cancer therapy. Cancer Research 58 (7), 1408–1416.

Brown, J. M., Wilson, W. R., 2004. Exploiting tumour hypoxia in cancer treatment. Nature Reviews Cancer 4 (6), 437–447.

Busse, J.-E., Gwiazda, P., Marciniak-Czochra, A., 2016. Mass concentration in a nonlocal model of clonal selection. Journal of mathematical biology 73 (4), 1001–1033.

Byrne, H., Drasdo, D., 2009. Individual-based and continuum models of growing cell populations: a comparison. Journal of Mathematical Biology 58 (4-5), 657–687.

Byrne, H. M., Chaplain, M., 1996. Growth of necrotic tumors in the presence and absence of inhibitors. Mathematical Biosciences 135 (2), 187–216.

Calabresi, P., Schein, P. S., Rosenberg, S. A., 1985. Medical oncology: basic principles and clinical management of cancer. MacMillan Pub. Co., New York, NY.

Casciari, J. J., Sotirchos, S. V., Sutherland, R. M., 1992. Variations in tumor cell growth rates and metabolism with oxygen concentration, glucose concentration, and extracellular ph. Journal of Cellular Physiology 151 (2), 386–394.

Chisholm, R. H., Lorenzi, T., Lorz, A., Larsen, A. K., De Almeida, L. N., Escargueil, A., Clairambault, J., 2015. Emergence of drug tolerance in cancer cell populations: an evolutionary outcome of selection, nongenetic instability, and stress-induced adaptation. Cancer Research 75 (6), 930–939.

Delitala, M., Lorenzi, T., 2012. A mathematical model for the dynamics of cancer hepatocytes under therapeutic actions. Journal of theoretical biology 297, 88–102.

Ding, L., Ellis, M. J., Li, S., Larson, D. E., Chen, K., Wallis, J. W., Harris, C. C., McLellan, M. D., Fulton, R. S., Fulton, L. L., Abbott, R. M., Hoog, J., Dooling, D. J., Koboldt, D. C., Schmidt, H., Kalicki, J., Zhang, Q., Chen, L., Lin, L., Wendl, M. C., McMichael, J. F., Magrini, V. J., Cook, L., McGrath, S. D., Vickery, T. L., Appelbaum, E., Deschryver, K., Davies, S., Guintoli, T., Lin, L., Crowder, R., Tao, Y., Snider, J. E., Smith, S. M., Dukes, A. F., Sanderson, G. E., Pohl, C. S., Delehaunty, K. D., Fronick, C. C., Pape, K. A., Reed, J. S., Robinson, J. S., Hodges, J. S., Schierding, W., Dees, N. D., Shen, D., Locke, D. P., Wiechert, M. E., Eldred, J. M., Peck, J. B., Oberkfell, B. J., Lolofie, J. T., Du, F., Hawkins, A. E., O'Laughlin, M. D., Bernard, K. E., Cunningham, M., Elliott, G., Mason, M. D., Thompson, D. M., Ivanovich, J. L., Goodfellow, P. J., Perou, C. M., Weinstock, G. M., Aft, R., Watson, M., Ley, T. J., Wilson, R. K., Mardis, E. R., Apr 2010. Genome remodelling in a basal-like breast cancer metastasis and xenograft. Nature 464 (7291), 999–1005.

Durand, R. E., Raleigh, J. A., 1998. Identification of nonproliferating but viable hypoxic tumor cells in vivo. Cancer Research 58 (16), 3547–3550.

Fu, F., Nowak, M. A., Bonhoeffer, S., 2015. Spatial heterogeneity in drug

concentrations can facilitate the emergence of resistance to cancer therapy. PLoS Computational Biology 11 (3), e1004142.

Gatenby, R. A., Silva, A. S., Gillies, R. J., Frieden, B. R., 2009. Adaptive therapy. Cancer Research 69 (11), 4894–4903.

Gerlinger, M., Rowan, A. J., Horswell, S., Larkin, J., Endesfelder, D., Gronroos, E., Martinez, P., Matthews, N., Stewart, A., Tarpey, P., et al., 2012. Intratumor heterogeneity and branched evolution revealed by multiregion sequencing. New England Journal of Medicine 366 (10), 883–892.

Gillies, R. J., Verduzco, D., Gatenby, R. A., 2012. Evolutionary dynamics of carcinogenesis and why targeted therapy does not work. Nature Reviews Cancer 12 (7), 487–493.

Gordan, J. D., Bertout, J. A., Hu, C.-J., Diehl, J. A., Simon, M. C., 2007. Hif-2α promotes hypoxic cell proliferation by enhancing c-myc transcriptional activity. Cancer Cell 11 (4), 335–347.

Greaves, M., Maley, C. C., 2012. Clonal evolution in cancer. Nature 481 (7381), 306–313.

Hlatky, L., Alpen, E., 1985. Two-dimensional diffusion limited system for cell growth. Cell Proliferation 18 (6), 597–611.

Hoefflin, R., Lahrmann, B., Warsow, G., Hübschmann, D., Spath, C., Walter, B., Chen, X., Hofer, L., Macher-Goeppinger, S., Tolstov, Y., et al., 2016. Spatial niche formation but not malignant progression is a driving force for intratumoural heterogeneity. Nature Communications 7.

Ibrahim-Hashim, A., Robertson-Tessi, M., Enrizues-Navas, P., Damaghi, M., Balagurunathan, Y., Wojtkowiak, J. W., Russell, S., Yoonseok, K., Lloyd, M. C., Bui, M. M., Brown, J. S., Anderson, A. R., Gillies, R. J., Gatenby, R. A., Mar 2017. Defining cancer subpopulations by adaptive strategies rather than molecular properties provides novel insights into intratumoral evolution. Cancer Res.

Jacqueline, C., Biro, P. A., Beckmann, C., Moller, A. P., Renaud, F., Sorci, G., Tasiemski, A., Ujvari, B., Thomas, F., Mar 2017. Cancer: A disease at the crossroads of trade-offs. Evol Appl 10 (3), 215–225.

Jones, A. M., Mitter, R., Springall, R., Graham, T., Winter, E., Gillett, C., Hanby, A. M., Tomlinson, I. P., Sawyer, E. J., Walker, R., Pinder, S., Jones, L., Ellis, I., Tan, P. H., Macartney, J., Green, D., Hales, S., Harding-Mackean, C., Colclough, A., MacNeill, F., Rowlands, D., Smith, C., Fentiman, I., Cane, P., Desai, A., Goderya, R., Nerurkar, A., Kissin, M., Jackson, P., Apr 2008. A comprehensive genetic profile of phyllodes tumours of the breast detects important mutations, intra-tumoral genetic heterogeneity and new genetic changes on recurrence. J. Pathol. 214 (5), 533–544.

Kumosa, L. S., Routh, T. L., Lin, J. T., Lucisano, J. Y., Gough, D. A., 2014. Permeability of subcutaneous tissues surrounding long-term implants to oxygen. Biomaterials 35 (29), 8287–8296.

Kwok, T., Twentyman, P., 1985. The response to cytotoxic drugs of emt6 cells treated either as intact or disaggregated spheroids. British Journal of Cancer 51 (2), 211.

Lavi, O., Greene, J. M., Levy, D., Gottesman, M. M., 2013. The role of cell density and intratumoral heterogeneity in multidrug resistance. Cancer research 73 (24), 7168–7175.

Levin, V. A., Patlak, C. S., Landahl, H. D., 1980. Heuristic modeling of drug delivery to malignant brain tumors. Journal of Pharmacokinetics and Biopharmaceutics 8 (3), 257–296.

Li, C. K., 1982. The glucose distribution in 9l rat brain multicell tumor spheroids and its effect on cell necrosis. Cancer 50 (10), 2066–2073.

Lloyd, M. C., Cunningham, J. J., Bui, M. M., Gillies, R. J., Brown, J. S., Gatenby, R. A., 2016. Darwinian dynamics of intratumoral heterogeneity: not solely random mutations but also variable environmental selection forces. Cancer Research 76 (11), 3136–3144.

Lopez, J. S., Banerji, U., 2016. Combine and conquer: challenges for targeted therapy combinations in early phase trials. Nature Reviews Clinical Oncology.

Lorenzi, T., Chisholm, R. H., Clairambault, J., 2016. Tracking the evolution of cancer cell populations through the mathematical lens of phenotype-structured equations. Biology Direct 11 (1), 43.

Lorenzi, T., Lorz, A., Perthame, B., 2017. On interfaces between cell populations with different mobilities. Kinetic and Related Models 10 (1), 299–311.

Lorz, A., Lorenzi, T., Clairambault, J., Escargueil, A., Perthame, B., 2015. Modeling the effects of space structure and combination therapies on phenotypic heterogeneity and drug resistance in solid tumors. Bulletin of Mathematical Biology 77 (1), 1–22.

Lorz, A., Lorenzi, T., Hochberg, M. E., Clairambault, J., Perthame, B., 2013. Populational adaptive evolution, chemotherapeutic resistance and multiple anti-cancer therapies. ESAIM: Mathematical Modelling and Numerical Analysis 47 (2), 377–399.

Macklin, P., McDougall, S., Anderson, A. R., Chaplain, M. A., Cristini, V., Lowengrub, J., 2009. Multiscale modelling and nonlinear simulation of vascular tumour growth. Journal of Mathematical Biology 58 (4-5), 765–798.

Martinez, P., Birkbak, N. J., Gerlinger, M., McGranahan, N., Burrell, R. A., Rowan, A. J., Joshi, T., Fisher, R., Larkin, J., Szallasi, Z., Swanton, C., Aug 2013. Parallel evolution of tumour subclones mimics diversity between tumours. J. Pathol. 230 (4), 356–364.

Marusyk, A., Almendro, V., Polyak, K., 2012. Intra-tumour heterogeneity: a looking glass for cancer? Nature Reviews Cancer 12 (5), 323–334.

Meads, M. B., Gatenby, R. A., Dalton, W. S., 2009. Environment-mediated drug resistance: a major contributor to minimal residual disease. Nature Reviews Cancer 9 (9), 665–674.

Melicow, M. M., 1982. The three steps to cancer: a new concept of cancerigenesis. Journal of Theoretical Biology 94 (2), 471–511.

Merlo, L. M., Pepper, J. W., Reid, B. J., Maley, C. C., 2006. Cancer as an evolutionary and ecological process. Nature Reviews Cancer 6 (12), 924–935.

Mirrahimi, S., Perthame, B., 2015. Asymptotic analysis of a selection model with space. Journal de Mathématiques Pures et Appliquées 104 (6), 1108–1118.

Norris, E., King, J. R., Byrne, H. M., 2006. Modelling the response of spatially structured tumours to chemotherapy: Drug kinetics. Mathematical and Computer Modelling 43 (7), 820–837.

Otwinowski, J., Plotkin, J. B., 2014. Inferring fitness landscapes by regression produces biased estimates of epistasis. Proceedings of the National Academy of Sciences 111 (22), E2301–E2309.

Perthame, B., 2006. Transport equations in biology. Springer Science & Business Media.

Perthame, B., Quirós, F., Vázquez, J. L., 2014. The hele–shaw asymptotics for mechanical models of tumor growth. Archive for Rational Mechanics and Analysis 212 (1), 93–127.

Pienta, K. J., McGregor, N., Axelrod, R., Axelrod, D. E., 2008. Ecological therapy for cancer: defining tumors using an ecosystem paradigm suggests new opportunities for novel cancer treatments. Translational Oncology 1 (4), 158–164.

Powathil, G. G., Gordon, K. E., Hill, L. A., Chaplain, M. A., 2012. Modelling the effects of cell-cycle heterogeneity on the response of a solid tumour to chemotherapy: biological insights from a hybrid multiscale cellular automaton model. Journal of Theoretical Biology 308, 1–19.

Pribluda, A., Cecile, C., Jackson, E. L., 2015. Intratumoral heterogeneity: from diversity comes resistance. Clinical Cancer Research 21 (13), 2916–2923.

Robertson-Tessi, M., Gillies, R. J., Gatenby, R. A., Anderson, A. R., 2015. Impact of metabolic heterogeneity on tumor growth, invasion, and treatment outcomes. Cancer Research 75 (8), 1567–1579.

Schmidt, A., Siebert, K., 2005. Design of adaptive finite element software: The finite element toolbox ALBERTA. Springer Verlag.

Schwarz, R. F., Ng, C. K., Cooke, S. L., Newman, S., Temple, J., Piskorz, A. M., Gale, D., Sayal, K., Murtaza, M., Baldwin, P. J., Rosenfeld, N., Earl, H. M., Sala, E., Jimenez-Linan, M., Parkinson, C. A., Markowetz,

F., Brenton, J. D., Feb 2015. Spatial and temporal heterogeneity in high-grade serous ovarian cancer: a phylogenetic analysis. PLoS Med. 12 (2), e1001789.

Sottoriva, A., Spiteri, I., Piccirillo, S. G., Touloumis, A., Collins, V. P., Marioni, J. C., Curtis, C., Watts, C., Tavare, S., Mar 2013. Intratumor heterogeneity in human glioblastoma reflects cancer evolutionary dynamics. Proc. Natl. Acad. Sci. U.S.A. 110 (10), 4009–4014.

Strese, S., Fryknäs, M., Larsson, R., Gullbo, J., 2013. Effects of hypoxia on human cancer cell line chemosensitivity. BMC Cancer 13 (1), 1.

Sullivan, R., Paré, G. C., Frederiksen, L. J., Semenza, G. L., Graham, C. H., 2008. Hypoxia-induced resistance to anticancer drugs is associated with decreased senescence and requires hypoxia-inducible factor-1 activity. Molecular Cancer Therapeutics 7 (7), 1961–1973.

Tang, M., Vauchelet, N., Cheddadi, I., Vignon-Clementel, I., Drasdo, D., Perthame, B., 2013. Composite waves for a cell population system modeling tumor growth and invasion. Chinese Annals of Mathematics, Series B 34 (2), 295–318.

Tannock, I., 1968. The relation between cell proliferation and the vascular system in a transplanted mouse mammary tumour. British Journal of Cancer 22 (2), 258.

Trédan, O., Galmarini, C. M., Patel, K., Tannock, I. F., 2007. Drug resistance and the solid tumor microenvironment. Journal of the National Cancer Institute 99 (19), 1441–1454.

Vermeulen, L., Morrissey, E., van der Heijden, M., Nicholson, A. M., Sottoriva, A., Buczacki, S., Kemp, R., Tavaré, S., Winton, D. J., 2013. Defining stem cell dynamics in models of intestinal tumor initiation. Science 342 (6161), 995–998.

Walther, V., Hiley, C. T., Shibata, D., Swanton, C., Turner, P. E., Maley, C. C., May 2015. Can oncology recapitulate paleontology? Lessons from species extinctions. Nat Rev Clin Oncol 12 (5), 273–285.

Wang, Y., Waters, J., Leung, M. L., Unruh, A., Roh, W., Shi, X., Chen, K., Scheet, P., Vattathil, S., Liang, H., et al., 2014. Clonal evolution in breast

cancer revealed by single nucleus genome sequencing. Nature 512 (7513), 155–160.

Ward, J. P., King, J., 1997. Mathematical modelling of avascular-tumour growth. Mathematical Medicine and Biology 14 (1), 39–69.

Wartenberg, M., Ling, F. C., Müschen, M., Klein, F., Acker, H., Gassmann, M., Petrat, K., Pütz, V., Hescheler, J., Sauer, H., 2003. Regulation of the multidrug resistance transporter p-glycoprotein in multicellular tumor spheroids by hypoxia-inducible factor (hif-1) and reactive oxygen species. The FASEB Journal 17 (3), 503–505.

Williams, M. J., Werner, B., Barnes, C. P., Graham, T. A., Sottoriva, A., Mar 2016. Identification of neutral tumor evolution across cancer types. Nat. Genet. 48 (3), 238–244.

Xia, T., Cheng, H., Zhu, Y., 2014. Knockdown of hypoxia-inducible factor-1 alpha reduces proliferation, induces apoptosis and attenuates the aggressive phenotype of retinoblastoma weri-rb-1 cells under hypoxic conditions. Annals of Clinical & Laboratory Science 44 (2), 134–144.

Yap, T. A., Gerlinger, M., Futreal, P. A., Pusztai, L., Swanton, C., 2012. Intratumor heterogeneity: seeing the wood for the trees. Science Translational Medicine 4 (127), 127ps10–127ps10.

Zhang, J., Fujimoto, J., Zhang, J., Wedge, D. C., Song, X., Zhang, J., Seth, S., Chow, C. W., Cao, Y., Gumbs, C., Gold, K. A., Kalhor, N., Little, L., Mahadeshwar, H., Moran, C., Protopopov, A., Sun, H., Tang, J., Wu, X., Ye, Y., William, W. N., Lee, J. J., Heymach, J. V., Hong, W. K., Swisher, S., Wistuba, I. I., Futreal, P. A., Oct 2014a. Intratumor heterogeneity in localized lung adenocarcinomas delineated by multiregion sequencing. Science 346 (6206), 256–259.

Zhang, X., Fryknäs, M., Hernlund, E., Fayad, W., De Milito, A., Olofsson, M. H., Gogvadze, V., Dang, L., Påhlman, S., Schughart, L. A. K., et al., 2014b. Induction of mitochondrial dysfunction as a strategy for targeting tumour cells in metabolically compromised microenvironments. Nature Communications 5.

Zhao, Y., Butler, E. B., Tan, M., 2013. Targeting cellular metabolism to improve cancer therapeutics. Cell Death & Disease 4 (3), e532.